Scaling laws for external fluid flow induced by controlled periodic heating of a solid boundary

Debashis Pal[1] and Suman Chakraborty[2,*]

[1]*Department of Aerospace Engineering and Applied Mechanics, Indian Institute of Engineering Science and Technology Shibpur, Howrah 711103, India*

[2]*Department of Mechanical Engineering, Indian Institute of Technology Kharagpur, Kharagpur 721302, India*

(Received 31 July 2019; revised manuscript received 12 January 2020; accepted 10 February 2020; published 11 March 2020)

We demonstrate that considerable variation of mean Prandtl number (Pr_0) from unity brings in an additional length scale (called the viscous penetration depth, δ_v) into the dynamics of instantaneous as well as time-averaged (mean) flow induced by thermoviscous expansion along a periodically heated solid wall. We investigate the limiting cases of high and low Prandtl numbers ($Pr_0 \gg 1$ and $Pr_0 \ll 1$) through detailed order-of-magnitude analysis. Our study reveals that the viscous penetration depth scales universally with Pr_0 so long as such depth remains small compared to the wavelength of the applied thermal wave. While a high Pr_0 is found to obstruct the mean flow, the converse is not necessarily true. Subsequent analysis clearly shows that a low-Pr_0 flow can induce negative thermoviscous force within the thermal boundary layer and thus retard the mean motion, leading to a nontrivial reduction of net mass flow along the plate. Numerical prediction of friction factor variation with Pr_0 agrees well with the scaling estimates for both high-Pr_0 and low-Pr_0 fluids. The findings may very well act as fundamental design basis for engineering devices that may potentially be developed for thermal molecular trapping and particle sorting and accumulation based on unsteady heating.

DOI: 10.1103/PhysRevE.101.033105

I. INTRODUCTION

Manipulation of transport processes using "unconventional" flow-actuation methods is central to the research and development of miniaturized fluidic devices [1–16], as they often prove superior to conventional methods of flow generation. The prospects of obtaining sustainable fluid motion through controlled external heating have been studied extensively in this regard [17–24], with a pioneering work by Weinert *et al.* [20] exploring possibilities of flow generation by virtue of thermoviscous expansion. Thermoviscous expansion of a liquid along a periodically heated wall constitutes a novel and intriguing thermo-mechanical pumping method that is capable of inducing net fluidic transport along the wall [20,25]. When a temperature wave travels along a wall in contact with a liquid, it alters the density as well as the viscosity of the adjacent liquid in a spatiotemporally evolving manner. Periodic thermal (volumetric) expansion and contraction close to the wall generate pressure pulsation, which triggers a fluctuating fluid motion. As the fluid is driven through periodically altering hot regions (low viscosity) and cold regions (high viscosity), the induced local velocity experiences a difference in magnitude that is synchronized with the variation of local viscosity (see Fig. 1). The difference in the magnitude of positive and negative velocity parallel to the wall eventually gives rise to a net flow opposite to the motion of the thermal wave, in a time-averaged sense.

It is necessary to acknowledge that fluid flow induced by thermoviscous actuation along a traveling thermal wave is essentially a multiscale transport phenomenon. Periodic fluctuation of temperature and associated thermoviscous actuation are usually confined to a "thin" thermal boundary layer which is characterized by a unique thermal penetration length scale (δ_t). The exact thickness of this thermal boundary layer and its detailed structure (i.e., two sublayers based on phase difference of local temperature) are provided in our previous work [25]. In narrow confinements such as microchannels, periodic thermoviscous expansion can induce a large variety of net velocity profiles (from uniform to parabolic) depending on the ratio of channel height to thermal penetration length [26]. The effect of thermoviscous expansion has been analyzed extensively in the field of microchannel acoustofluidics over the past few years. Rednikov and Sadhal [27] analytically showed that the contribution of the nonadiabatic thermoviscous effect (which becomes apparent through fluctuating density and viscosity perturbations) to acoustic streaming is indeed significant for liquids. Recent studies have shown interesting results in the application of the temperature-induced thermoviscous effect in controlling acoustic radiation force and boundary-driven acoustic streaming in a long straight microfluidic channel containing a Newtonian fluid [28,29]. Nevertheless, implications of such periodically fluctuating flow may also be far ranging, opening up possibilities of obtaining significant progress in the development of contactless thermal trapping and sorting devices [30,31], in microcombustion and power generation applications [32–34], and in micromixing and separation processes [35,36]. A noteworthy limitation of existing literature on thermoviscous actuation [20,25–29] is that they are focused on fluids having Prandtl number close to unity. In reality, Prandtl number varies with the fluid as well as with temperature.

The present work explores the consequences of Prandtl number variation on flow induced by thermoviscous

*suman@mech.iitkgp.ernet.in

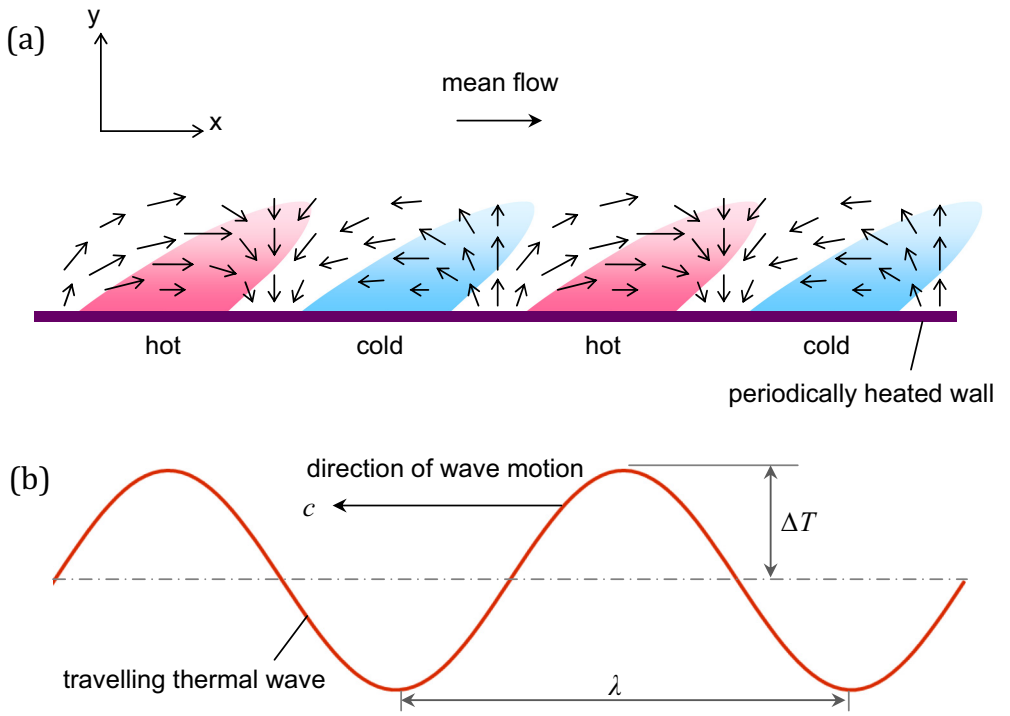

FIG. 1. (a) Instantaneous flow field induced by thermoviscous expansion along a traveling temperature wave applied on a flat plate. Two consecutive cycles with periodically altering hot (red) and cold (blue) regions are portrayed. Positive and negative x velocities (parallel to the plate) exhibit difference in magnitude (arrow length) between the hot and cold regions. Resulting mean or time averaged flow direction is also shown. (b) Temperature wave, traveling along the plate with constant speed c from right to left.

expansion in an unconfined configuration, i.e., flow over a flat plate. When the mean Prandtl number (Pr_0) deviates significantly from unity, an additional length scale (viscous penetration depth or characteristic thickness of the viscous boundary layer) starts influencing the concerned dynamics of instantaneous as well as time-averaged (mean) flow. Accordingly, the limiting cases of high and low Prandtl numbers ($\mathrm{Pr}_0 \gg 1$ and $\mathrm{Pr}_0 \ll 1$) are investigated through detailed scaling analysis of equations of motion (both instantaneous and mean motion). The theoretical analysis is corroborated by full-scale computational fluid dynamics (CFD) simulations of governing transport equations: continuity, Navier-Stokes, and energy conservation.

There are three main contributions in this paper. First, we appropriately define a viscous boundary layer which is characterized by a length scale called viscous penetration depth (δ_v) and show that the ratio of viscous penetration depth to thermal penetration length (δ_v/δ_t) scales as $\sqrt{\mathrm{Pr}}$. An exception to this scaling law is also observed for very high Prandtl number (owing to an elevated viscosity), wherein the wavelength of the thermal wave (λ) curbs the growth of viscous boundary layer and the dependence of δ_v/δ_t on the Prandtl number weakens substantially. Second, we deduced the physical scales for time-averaged velocity and friction factor for the limiting cases of high and low Prandtl numbers ($\mathrm{Pr}_0 \gg 1$ and $\mathrm{Pr}_0 \ll 1$), and subsequently corroborated them using CFD simulations. Numerical results demonstrate that such scales are valid for Prandtl numbers that are moderately higher and lower than unity ($\mathrm{Pr}_0 > 1$ and $\mathrm{Pr}_0 < 1$) as well, extending their range of applicability. These scaling laws may turn into important design criteria for devices developed for thermal trapping, accumulation, and sorting of particles and biomolecules in a micro-scale confinement. Finally, the most intriguing outcome of this study is that while a large Pr_0 is found to hinder the mean flow, the converse is not necessarily true as a small Pr_0 can also retard the mean motion by inducing negative thermoviscous force within the thermal boundary layer itself. We exemplify how a low-Pr_0 flow, unlike the cases of forced or free convection, yields a net mass flow much less than the expected value. Such a result is indeed a nontrivial one as it is likely that for large Pr_0 viscous friction would dominate over thermal diffusion leading to low flow rate, whereas for small Pr_0 viscous resistance would be weaker so that the flow rates would be higher.

II. PROBLEM DESCRIPTION AND GOVERNING EQUATIONS

The geometry under consideration consists of a long flat plate aligned with the x axis and in contact with an infinite expanse of fluid ($0 < y < \infty$), as shown in Fig. 1(a). Initially, the fluid is at rest and at a constant temperature T_0. In order to generate fluid motion, an unsteady thermal boundary condition in form of a sinusoidal temperature wave is applied along the plate [see Fig. 1(b)]. Amplitude, wavelength, and speed of propagation of the thermal wave are ΔT, λ, and c, respectively. Thus, the thermal boundary condition is aptly expressed as

$$T_{\mathrm{wall}} = T_0 + \Delta T \cos\left\{\frac{2\pi}{\lambda}(x + ct)\right\}. \tag{1}$$

Equation (1) straightway gives us a few important scales such as the characteristic temperature-difference scale ΔT, the length scale λ over which temperature varies in the x direction, and the periodic time scale λ/c $(=t_u)$. As the thermal wave travels along the wall, the temperature of the fluid near the wall fluctuates periodically in space (x) and time. The subsequent thermal expansion-compression of the fluid generates a velocity field that is also periodic in time as well as in streamwise direction (x). Thus, even though the flow is "incompressible," an equation of state dictating the spatiotemporal variation of density is required along with usual flow governing equations. Considering two-dimensional nature of the problem, the flow-governing equations—continuity, Navier-Stokes, and energy equations—are expressed as

$$\frac{\partial \rho}{\partial t} + \frac{\partial}{\partial x}(\rho u) + \frac{\partial}{\partial y}(\rho v) = 0, \tag{2}$$

$$\rho\left[\frac{\partial u}{\partial t} + u\frac{\partial u}{\partial x} + v\frac{\partial u}{\partial y}\right] = -\frac{\partial p}{\partial x} + \frac{\partial}{\partial x}\left[2\mu\left(\frac{\partial u}{\partial x} - \frac{1}{3}\nabla\cdot\vec{V}\right)\right] + \frac{\partial}{\partial y}\left[\mu\left(\frac{\partial u}{\partial y} + \frac{\partial v}{\partial x}\right)\right], \tag{3a}$$

$$\rho\left[\frac{\partial v}{\partial t} + u\frac{\partial v}{\partial x} + v\frac{\partial v}{\partial y}\right] = -\frac{\partial p}{\partial y} + \frac{\partial}{\partial x}\left[\mu\left(\frac{\partial v}{\partial x} + \frac{\partial u}{\partial y}\right)\right] + \frac{\partial}{\partial y}\left[2\mu\left(\frac{\partial v}{\partial y} - \frac{1}{3}\nabla\cdot\vec{V}\right)\right], \tag{3b}$$

$$\rho C_p\left[\frac{\partial T}{\partial t} + u\frac{\partial T}{\partial x} + v\frac{\partial T}{\partial y}\right] = \beta_T T\frac{Dp}{Dt} + \nabla\cdot(k\nabla T) + \Phi, \tag{4}$$

where p is pressure, T is temperature, and u and v are the x component and y component of flow velocity, respectively. Symbols ρ, μ, k, C_p, β_T, and Φ represent density, viscosity, thermal conductivity, constant pressure specific heat, thermal expansion coefficient, and viscous dissipation function, respectively. The volumetric thermal expansion coefficient (β_T) of liquids is typically a small quantity (in the range $\sim 10^{-3}$–10^{-4} K^{-1}). We consider the amplitude of the thermal wave to be small so that $\beta_T\,\Delta T \ll 1$. An equation of state for temperature-dependent density is prescribed by

$$\rho - \rho_0 = -\beta_T \rho_0 (T - T_0), \tag{5}$$

where both ρ_0 and β_T are evaluated at the reference state (T_0). Local viscosity may be evaluated by employing a linearized relation [20] similar to Eq. (5) as

$$\mu - \mu_0 = -\eta_T \mu_0 (T - T_0), \tag{6}$$

where μ_0 and η_T are the viscosity and thermal viscosity coefficient of the fluid in its reference state.

It is necessary to acknowledge that fluid flow induced by thermoviscous actuation along a traveling thermal wave is essentially a multiscale transport phenomenon. A major challenge in analyzing such a fluidic transport lies in figuring out the intricate interplay of various length scales involved. In the present problem, the temperature varies over a characteristic length λ in the x direction. In the transverse direction, however, the temperature variation is governed by a thermal diffusion length scale defined on basis of the periodic time scale, t_u $(=\lambda/c)$. Therefore, the y length scale for temperature variation (also called thermal penetration length) is prescribed by $\delta_t = \sqrt{\alpha_0 t_u}$, where α_0 is the thermal diffusivity of the fluid in its reference state (T_0). Such a length scale is essentially obtained by scaling the energy equation [Eq. (4)]. Based on the characteristic thickness δ_t, one can define a thermal boundary layer adjacent to the wall, wherein the entire thermal fluctuation and associated thermoviscous actuation remain confined. Detailed accounts of this thermal boundary layer (also known as the wall layer) and its sublayers are discussed elsewhere [25] and are not repeated here for the sake of brevity. Apart from λ and δ_t, an additional length scale associated with viscous diffusion may emerge as a key governing parameter, particularly if the Prandtl number deviates from unity. An important consideration of several previous works [20,25–29] is that the mean Prandtl number (Pr_0) of the fluid is chosen to be of order 1. The physical implication of $\mathrm{Pr}_0 \sim O(1)$ is that the length scales associated with viscous spreading and thermal spreading by diffusion process are of the same order. It is essential to recall that Pr_0 may differ considerably from unity not only due to a change of fluid but with an alteration of mean temperature (T_0) also. Appropriate scaling of the momentum equation [Eq. (3)] is likely to reveal the exact role of such a viscous diffusion length scale on the thermoviscous pumping phenomena. Here, we pinpoint the important considerations and assumptions involved in the present analysis:

(i) The plate is long, i.e., length $L \gg \lambda$.

(ii) Stokes's hypothesis is valid.

(iii) Thermal diffusivity is treated as a constant (evaluated at the mean temperature T_0).

(iv) Gravity (buoyancy effect) is neglected.

(v) In order to generate significant flow velocity, we need a steep temperature gradient and a substantial wave speed c. Therefore, we keep wavelength short, ∼50–200 μm, and maintain ΔT at least of order ∼10 K. The upper bound of ΔT depends on the freezing point and boiling point of a particular liquid (e.g., for water ΔT ∼10 K, for mercury ΔT ∼100 K, etc.). It is observed that a wave speed (c) of order ∼1 m/s yields the highest mean velocity (U_{avg}), of orders 50, 10, and 500 μm/s for $\mathrm{Pr}_0 \sim 1$, $\mathrm{Pr}_0 \gg 1$, and $\mathrm{Pr}_0 \ll 1$ fluids, respectively. Since the thermal diffusivity (α_0) is in the range $\sim 10^{-6}$–10^{-7} m^2/s (see Table II), with a typical wave speed of 1 m/s, wavelength λ turns out to be at least one order of magnitude greater than δ_t $(=\sqrt{\alpha_0 \lambda/c})$.

(vi) Thermal expansion coefficient β_T is small (a fact for most liquids), so that $\beta_T\,\Delta T \ll 1$ and density function $\rho(T)$ is evaluated from a linearized equation of state [Eq. (5)].

(vii) With $\beta_T\,\Delta T \ll 1$ and $\lambda \geqslant 10\,\delta_t$ it turns out that wave speed $c \gg u,\ v$. This result leads to great simplification of the continuity, momentum, and energy equations [Eqs. (2), (3), and (4)], as the convective transport of momentum as well as energy turns out to be negligible compared to respective unsteady terms $(\partial u/\partial t$ and $\partial T/\partial t)$. The continuity equation reduces to $\nabla\cdot\vec{V} \simeq \beta_T\,(\partial T/\partial t)$. These results are true for all Pr_0.

(viii) For large Pr_0, we assume that λ is at least one order of magnitude greater than the viscous diffusion length δ_{v}. This

assumption is not required for low-Pr_0 fluids, as δ_v itself is smaller than δ_t.

In the subsequent section, we focus on the consequences of Pr_0 variation on the instantaneous (oscillating) as well as the time-averaged (mean) flow induced by thermoviscous actuation. Since the oscillatory flow field does not yield the typical hydrodynamic boundary layer (observed in forced convection as well as natural convection) over a flat plate, a characteristic viscous spreading length or viscous penetration depth scale (δ_v) is defined at the outset. Then, the limiting cases of very high and very low Pr_0, which involve substantial difference in the spreading of viscous and thermal effects, are investigated through appropriate scaling of the pertinent governing equation [Eq. (3a)]. The estimated length scale δ_v and the mean velocity scale U_s are numerically corroborated for a wide range of mean Prandtl numbers. Our analysis further delineates how the intricate interplay of viscous penetration depth (δ_v) and thermal penetration length (δ_t) induces a nontrivial mean velocity profile near the wall for the limiting case of low Prandtl number flow ($\mathrm{Pr}_0 \ll 1$).

III. SCALING ANALYSIS

In an unconfined configuration, instantaneous x and y velocities induced by the thermal expansion of the fluid are of the same order (i.e., $u \sim v$). This is true irrespective of the mean Prandtl number (Pr_0) under concern. Therefore, the instantaneous velocity scale within the thermal boundary layer is determined [25] from a simplified version of continuity the equation [Eq. (2)] as

$$u_s \sim \beta_T \Delta T\, c\left(\frac{\delta_t}{\lambda}\right). \tag{7}$$

Scaling relation (7) confirms that with $\beta_T \Delta T \ll 1$ and λ considerably bigger than δ_t, wave speed is much greater than the instantaneous velocity scale, i.e. $c \gg u_s$. Since $\beta_T \Delta T \ll 1$, one can neglect the small density variation in the inertia term and substitute $\rho \approx \rho_0$ in the left hand side of the momentum balance equation [Eq. (3)].

A. Scaling of the *x*-momentum equation within the thermal boundary layer

Employing the linearized function for viscosity variation [Eq. (6)], we rearrange the x-momentum equation [Eq. (3a)] as

$$\begin{aligned}\rho_0\frac{Du}{Dt} = &-\frac{\partial p}{\partial x} + \mu_0\left[\left(\frac{\partial^2 u}{\partial x^2}+\frac{\partial^2 u}{\partial y^2}\right)+\frac{\partial}{\partial x}\left(\frac{\nabla\cdot\vec{V}}{3}\right)\right]\\ &-\mu_0\eta_T\left[\frac{\partial}{\partial x}\left\{2(T-T_0)\left(\frac{\partial u}{\partial x}-\frac{\nabla\cdot\vec{V}}{3}\right)\right\}\right.\\ &\left.+\frac{\partial}{\partial y}\left\{(T-T_0)\left(\frac{\partial u}{\partial y}+\frac{\partial v}{\partial x}\right)\right\}\right].\end{aligned} \tag{8}$$

Evidently, the second term on the right-hand side of Eq. (8), involving mean viscosity (μ_0), represents the usual viscous friction in a constant viscosity flow, while the last term (involving $\mu_0\eta_T$ and explicitly dependent of T) is a direct consequence of viscosity variation. This temperature-dependent variable friction term, instrumental in generating net unidirectional fluid motion, is aptly named "thermoviscous forcing." There is no externally applied pressure gradient in the flow domain. The passive pressure field is induced by unsteady fluctuation of temperature and velocity. Since the wave speed $c \gg u,\ v$, it turns out that the temporal acceleration is much larger than the convective acceleration. Therefore, the inertia term may be simplified as $\rho_0(Du/Dt) \approx \rho_0(\partial u/\partial t)$, and the scale representing inertia is given by the expression

$$\text{inertia}: \rho_0\frac{\partial u}{\partial t} \sim \frac{\rho_0 u_s}{t_u} = \frac{\rho_0\beta_T\Delta T c^2\delta_t}{\lambda^2}. \tag{9}$$

Considering δ_t as the y length scale within the thermal boundary layer region, we simplify the right-hand side of Eq. (8) further. Since the x length scale λ is considerably bigger than δ_t, we obtain the respective scales for viscous-friction and "thermoviscous forcing" terms as

$$\text{viscous friction}: \mu_0\frac{\partial^2 u}{\partial y^2} \sim \frac{\mu_0 u_s}{\delta_t^2} = \frac{\mu_0\beta_T\Delta T c}{\lambda\delta_t}, \tag{10}$$

thermoviscous forcing:

$$\mu_0\eta_T\frac{\partial}{\partial y}\left[(T-T_0)\frac{\partial u}{\partial y}\right] \sim \frac{\mu_0\eta_T\Delta T u_s}{\delta_t^2} = \frac{\mu_0\beta_T\eta_T\Delta T^2 c}{\lambda\delta_t}. \tag{11}$$

Thus, the x-momentum equation assumes a greatly simplified form within the wall layer, as

$$\rho_0\frac{\partial u}{\partial t} \approx -\frac{\partial p}{\partial x} + \mu_0\frac{\partial^2 u}{\partial y^2} - \mu_0\eta_T\frac{\partial}{\partial y}\left[(T-T_0)\frac{\partial u}{\partial y}\right]. \tag{12}$$

Recognizing the interplay among three main forces, one can recast them by dividing with the scale for viscous-friction and obtain

$$\underset{\text{inertia}}{\mathrm{Pr}_0^{-1}} \quad \underset{\text{friction}}{1} \quad \underset{\text{thermoviscous force}}{\eta_T\Delta T}. \tag{13}$$

From expression (13) it is clear that the competition between inertia and friction is dictated solely by a fluid property, the Prandtl number Pr_0 (evaluated at the mean temperature, T_0). While the friction term represents viscous resistance offered to the flow by way of mean viscosity (μ_0, a constant), it is crucial to understand that the so-called thermoviscous forcing is essentially the "variable friction" originating out of temperature dependence of the viscosity and, therefore, is instrumental in generating net (time-averaged) unidirectional flow. Relative strength of thermoviscous force and friction depends on the product of thermal viscosity coefficient (η_T, a fluid property) and amplitude of thermal wave, ΔT.

B. Viscous penetration depth scale

In thermoviscous expansion driven fluidic transport, viscous penetration depth scale (δ_v) characterizes a region wherein the viscous influence of wall is important in context of flow (velocity) oscillation. One may recall here that the oscillating x velocity (u) is zero at the wall boundary (no-slip condition). Far away from the wall ($y \to \infty$) u equals zero, too. Accordingly, we can define δ_v as the depth where the x-velocity component u reaches its peak value during a cycle

(since the flow itself is oscillating). Once the periodic "steady state" is achieved, this depth (δ_v) becomes invariant with time.

We know that thermoviscous actuation is present inside the wall layer (up to $y \sim \delta_t$) only. Next to the wall layer, there is a distinct region ($\delta_t < y < \lambda$) in which p, u, and v fluctuate with the same periodicity ($t_u = \lambda/c$) as that of the temperature wave but the temperature field itself remains uniform (i.e., $T = T_0$). This region is called the intermediate layer [25]. In the region $y \geqslant \lambda$ (outer layer), there is no fluctuation whatsoever. Thus, λ is the length scale for pressure and velocity variation not only in the x direction but in the y direction as well. Since the fluctuation in the x velocity, caused by successive expansion-contraction of the fluid and subsequent inertia, ceases at around $y \sim \lambda$, the x velocity (u) reaches its peak value somewhere in between $y = 0$ and $y = \lambda$. However, the distances from the wall where the velocity components u and v attain their maxima need not be the same. We recall that u and v both are induced primarily by thermal expansion-contraction. Therefore, the magnitude of v, which is zero at the wall, gradually increases with y up to a distance where significant temperature fluctuation is present. This distance is characterized by thermal penetration length δ_t, irrespective of the Prandtl number. In contrast, u is influenced by the local viscosity [see the schematic in Fig. 1(a), which is a very good qualitative representation of the actual flow field] and, quite intuitively, we expect that both the amplitude of oscillation of u and the location of maximum u would depend on the relative spreading of viscous and thermal effects.

For Prandtl number (Pr_0) close to unity, effects of viscous spreading and thermal spreading by diffusion are similar. Consequently, the viscous penetration depth δ_v and thermal penetration depth δ_t are of the same order. However, for $\mathrm{Pr}_0 \ll 1$ and $\mathrm{Pr}_0 \gg 1$, viscous penetration depth δ_v will be noticeably different from δ_t. In order to ascertain the scaling relationship between δ_v and δ_t, it is necessary to investigate the limiting cases of high Prandtl number and low Prandtl number flows extensively. In order to numerically validate the scaling laws for δ_v in Sec. III, we employ an averaged measure as follows. Once the periodic "steady state" is reached, we monitor the oscillation of u at any x location (fixed) and calculate δ_v as the average of y coordinates where the x velocity reaches its maxima (positive peak, $u^+_{\max}$) and minima (negative peak, $u^-_{\min}$) during a cycle (time period $t_u = \lambda/c$). Thus, δ_v is the distance up to which the amplitude of oscillation of the x velocity (u) increases; once we cross this point ($y > \delta_v$) oscillation of u decays gradually. In this regard, we acknowledge that it is the difference between positive and negative x velocity (i.e., $|u^+| - |u^-|$) that gives rise to the mean or time averaged flow. In subsequent discussion, henceforth, δ_v is also termed the characteristic thickness of the viscous boundary layer.

1. *Scaling for high Prandtl number* ($\mathrm{Pr}_0 \gg 1$)

It is evident that the thermal forcing (equivalent to expansion-contraction of the fluid) is confined within the thermal boundary layer region, which is characterized by the scale δ_t. When the mean Prandtl number (Pr_0) is much greater than unity, friction thoroughly dominates over inertia within the thermal boundary layer and it is possible for this layer to viscously entrain a layer of outer fluid. Such a viscously driven layer is characterized by the scale δ_v. For high-Pr_0 fluids, thus, the length scale associated with viscous diffusion is greater than that associated with thermal diffusion and, accordingly, one may assume $\delta_v \gg \delta_t$. Since the fluid outside the thermal boundary layer is unaffected by temperature fluctuation (i.e., $T \simeq T_0$), from Eqs. (2) and (8) one can deduce continuity and x-momentum equations for this viscous boundary layer of characteristic thickness δ_v as

$$\nabla \cdot \vec{V} = 0, \tag{14a}$$

$$\rho_0 \frac{\partial u}{\partial t} = -\frac{\partial p}{\partial x} + \mu_0 \left(\frac{\partial^2 u}{\partial x^2} + \frac{\partial^2 u}{\partial y^2} \right). \tag{14b}$$

In effect, the δ_v layer is driven viscously by a much thinner δ_t layer and is restrained by its own inertia. Therefore, a balance between inertia and friction force within the viscous boundary layer [Eq. (14b)] yields

$$\frac{\rho_0 u_s}{t_u} \sim \frac{\mu_0 u_s}{\delta_v^2}.$$

An inherent assumption in the above scaling is that the y length scale δ_v is at least one order of magnitude smaller than the x length scale λ. Substituting the periodic time scale $t_u = \lambda/c$, and making use of the definition of the thermal penetration length scale, δ_t ($=\sqrt{\alpha_0 \lambda/c}$), we obtain

$$\frac{\delta_v}{\delta_t} \sim \mathrm{Pr}_0^{1/2} > 1. \tag{15}$$

From the scaling prescribed by relation (15) it appears that the viscous boundary layer (thickness $\sim\delta_v$) can grow with the Prandtl number in an unbounded manner, which is, however, not possible. For a given wavelength λ, if we increase Pr_0 by increasing the viscosity μ_0 gradually, then the constraint on δ_v (to be at least one order of magnitude smaller than λ) will fail at some value of Pr_0. This is substantiated by our numerical solution in a subsequent section.

2. *Scaling for low Prandtl number* ($\mathrm{Pr}_0 \ll 1$)

For $\mathrm{Pr}_0 \ll 1$, thermal diffusivity of the fluid is much greater than its viscosity, and the thermal penetration length δ_t will be large compared to δ_v. It is not difficult to realize that there is an extremely "thin" viscous boundary layer adjacent to the wall, wherein friction is supposed to play an important role. Nevertheless, for a major part of the heated wall layer ($\delta_v < y < \delta_t$) inertia turns out to be a dominant force over friction. Thus, for low Prandtl number, there exists a thin thermal boundary layer (considering δ_t significantly smaller than λ) and a much thinner viscous boundary layer close to the wall. In order to resolve the near-wall region correctly, one has to scale the x-momentum equation [Eq. (8)] with the smallest length scale ($y_s = \delta_v$). The scales for instantaneous velocity (u_s) and inertia turn out to be same as those prescribed by expressions (7) and (9), respectively. However, within the viscous boundary layer region ($y \leqslant \delta_v$), friction and thermoviscous forcing terms yield different scales, as

$$\text{friction} : \mu_0 \frac{\partial^2 u}{\partial y^2} \sim \frac{\mu_0 u_s}{\delta_v^2} = \frac{\mu_0 \beta_T \Delta T c}{\lambda \delta_t} \left(\frac{\delta_t}{\delta_v} \right)^2, \tag{16a}$$

thermoviscous forcing:

$$\mu_0\eta_T\frac{\partial}{\partial y}\left[(T-T_0)\frac{\partial u}{\partial y}\right] \sim \frac{\mu_0\eta_T\Delta T u_s}{\delta_v^2} = \frac{\mu_0\beta_T\eta_T\Delta T^2 c}{\lambda\delta_t}\left(\frac{\delta_t}{\delta_v}\right)^2. \tag{16b}$$

Comparing inertia, friction and thermoviscous forcing terms, one may obtain a scaling relation for low-Pr fluids within $y \leqslant \delta_v$ as well:

$$\underset{\text{inertia}}{\mathrm{Pr}_0^{-1}\left(\frac{\delta_v}{\delta_t}\right)^2} \quad \underset{\text{friction}}{1} \quad \underset{\text{thermoviscous force}}{\eta_T\Delta T}. \tag{17}$$

Thus, for low Prandtl number ($\mathrm{Pr}_0 \ll 1$) fluids, inertia completely dominates over friction in the major part of the thermal boundary layer, irrespective of $\eta_T\Delta T$; however, close to the wall, where an extremely thin viscous boundary layer is formed, these two forces strike a balance (due to ${\delta_v}^2 \ll {\delta_t}^2$). A balance between inertia and friction in the viscous boundary layer implies

$$\frac{\delta_v}{\delta_t} \sim \mathrm{Pr}_0^{1/2} < 1. \tag{18}$$

The importance of thermoviscous force relative to viscous friction depends solely on $\eta_T\Delta T$. Outside the wall layer, thermoviscous force is absent, and inertia and friction balance each other.

C. Investigation of mean (time-averaged) flow

The time-averaged or mean velocities, U_{avg} and V_{avg}, are found by time averaging the instantaneous velocities, u and v, respectively, over a cycle (time period $t_u = \lambda/c$). Since the temperature field is uniform ($T = T_0$) and velocities are zero at $t = 0$, spreading of thermal energy and momentum in the transverse direction (by diffusion) requires some time to complete. At sufficiently large observation time, temperature and velocity oscillations in the thermal boundary layer become "periodically steady." Thus, once the initial transients have died, the flow field achieves a "periodic steady state" within the wall layer, which implies that the net or time-averaged velocity within the thermal boundary layer does not vary with t or x anymore. The governing equation for the mean flow may now be deduced [25] by time averaging the x-momentum equation [Eq. (8)] over a complete cycle as

$$\frac{\partial^2 U_{\mathrm{avg}}}{\partial y^2} = \eta_T\frac{\partial}{\partial y}\left[\overline{(T-T_0)\left(\frac{\partial u}{\partial y}+\frac{\partial v}{\partial x}\right)}\right], \tag{19}$$

where the overbar denotes time average over a time period $t_u = \lambda/c$.

1. Mean velocity scale for high Prandtl number ($\mathrm{Pr}_0 \gg 1$)

For a high Prandtl number flow, characteristic thickness of the viscous boundary layer scales as $\delta_v \sim \sqrt{\mathrm{Pr}_0}\,\delta_t$. We know that such a scaling is valid only when δ_v is smaller than λ by at least one order of magnitude. Since $\delta_t < \delta_v$, velocity derivative $\partial u/\partial y$ in the thermal boundary layer scales as

$$\frac{\partial u}{\partial y} \sim \frac{u_s}{\delta_v} = \frac{u_s}{\sqrt{\mathrm{Pr}_0}\,\delta_t}. \tag{20}$$

The appropriate y length scale for the mean velocity (U_{avg}) induced by thermoviscous actuation within the thermal boundary layer is δ_t. Substituting relevant scales in the governing equation for time-averaged flow [Eq. (19)], we therefore obtain

$$\frac{U_s}{{\delta_t}^2} \sim \frac{\eta_T\Delta T}{\delta_t}\left(\frac{u_s}{\sqrt{\mathrm{Pr}_0}\,\delta_t}+\frac{u_s}{\lambda}\right).$$

Unless Pr_0 is too large, $\delta_v \sim \sqrt{\mathrm{Pr}_0}\,\delta_t$ remains considerably smaller than λ. Thus, the mean or net velocity scale for high-Pr_0 flows is prescribed by

$$U_s \sim \frac{\eta_T\Delta T\, u_s}{\sqrt{\mathrm{Pr}_0}} = \beta_T\eta_T\,(\Delta T)^2\alpha_0\left(\frac{c}{\nu_0\lambda}\right)^{0.5}. \tag{21}$$

The dependence of mean velocity upon the Prandtl number [or, the kinematic viscosity ν_0 as shown in Eq. (21)] is the hallmark of high Prandtl number flow driven by thermoviscous expansion. Equation (21) implies that higher the viscosity is (compared to thermal conductivity), the less will be the net volumetric throughput. In a subsequent section, it is numerically demonstrated that the mean velocity scale predicted by (21) is applicable to not just the limiting cases of $\mathrm{Pr}_0 \gg 1$ but also to any fluid having $\mathrm{Pr}_0 \geqslant 1$. This is somewhat anticipated as the scaling relation (21), for $\mathrm{Pr}_0 = 1$, yields the mean velocity scale of $\mathrm{Pr}_0 \sim O(1)$ flow (expression (19); cf. [25]).

2. Mean velocity scale for low Prandtl number ($\mathrm{Pr}_0 \ll 1$)

For a low Prandtl number flow, the viscous boundary layer ($\sim\delta_v$) is considerably thinner than the thermal boundary layer ($\sim\delta_t$). Thus, within the thermal boundary layer, two distinct regions coexist: (a) a viscous boundary layer ($y \leqslant \delta_v$) wherein local velocity gradient $\partial u/\partial y$ scales as $\sim u_s/\delta_v$, and (b) a region outside the viscous boundary layer but inside the thermal boundary layer ($\delta_v < y \leqslant \delta_t$) wherein $\partial u/\partial y$ does not scale as u_s/δ_v [also evident from Fig. 2(d)]. In both these regions, however, thermoviscous forcing remains significant. Since the scale representing $\partial u/\partial y$ is known, the mean velocity scale within the viscous boundary layer region (adjacent to the wall) can be estimated from Eq. (19). The appropriate length scale for the mean velocity field within the viscous boundary layer is δ_v ($\sim\sqrt{\mathrm{Pr}_0}\,\delta_t$) too. Therefore, Eq. (19) yields

$$\frac{U_s}{{\delta_v}^2} \sim \frac{\eta_T\Delta T}{\delta_v}\left(\frac{u_s}{\sqrt{\mathrm{Pr}_0}\,\delta_t}+\frac{u_s}{\lambda}\right).$$

Since δ_t is at least one order smaller than λ and $\mathrm{Pr}_0 \ll 1$, the above expression assumes the form

$$U_s \sim \eta_T\Delta T\, u_s = \beta_T\eta_T\,(\Delta T)^2\left(\frac{\alpha_0\, c}{\lambda}\right)^{0.5}. \tag{22}$$

Even though the mean velocity scale [Eq. (22)] appears exactly same as that of the $\mathrm{Pr}_0 \sim O(1)$ flow (expression (19); cf. [25]), the difference lies in the region where they are applicable. While the expression (19) from [25] is valid for the entire thermal boundary layer region, Eq. (22) is valid within the considerably thinner viscous boundary layer ($y \leqslant \delta_v$) only.

TABLE I. Various physical scales deduced in this work.

	$\mathrm{Pr}_0 \gg 1$	$\mathrm{Pr}_0 \ll 1$
Ratio of viscous penetration depth to thermal penetration length	$\frac{\delta_v}{\delta_t} \sim \mathrm{Pr}_0^{1/2}$	$\frac{\delta_v}{\delta_t} \sim \mathrm{Pr}_0^{1/2}$
Scales for time-averaged (mean) velocity	$U_s \sim \beta_T \eta_T (\Delta T)^2 \alpha_0 \left(\frac{c}{v_0 \lambda}\right)^{0.5}$	$U_s \sim \beta_T \eta_T (\Delta T)^2 \left(\frac{\alpha_0 c}{\lambda}\right)^{0.5}$
Time-averaged wall shear (dimensionless)	$\bar{\tau}_w \sim \frac{\mathrm{Pr}_0^{3/2}}{\beta_T \eta_T (\Delta T)^2}$	$\bar{\tau}_w \sim \frac{\mathrm{Pr}_0^{1/2}}{\beta_T \eta_T (\Delta T)^2}$

D. Scaling estimates for friction factor

Appropriate scales for the friction factor (dimensionless wall shear) may be deduced using the length scales and mean velocity scales for high-Pr_0 and low-Pr_0 cases. We know that the time-averaged wall shear stress scales as

$$(\tau_w)_{\mathrm{avg}} \equiv \mu_0 \left.\frac{dU_{\mathrm{avg}}}{dy}\right|_w \sim \frac{\mu_0 U_s}{y_s}$$

When Pr_0 is much greater than unity, the length scale is $y_s \sim \delta_t$ and the mean velocity scale U_s is prescribed by expression (21). Therefore, the friction factor varies as

$$\bar{\tau}_w = \frac{(\tau_w)_{\mathrm{avg}}}{\rho_0 U_s^2} \sim \frac{\nu_0}{U_s\, \delta_t} \sim \frac{\nu_0 \sqrt{\mathrm{Pr}_0}}{\eta_T\, \Delta T\, u_s\, \delta_t} \sim \frac{\mathrm{Pr}_0^{3/2}}{\beta_T\, \eta_T\, (\Delta T)^2}. \tag{23}$$

The opposite limit, i.e., a low-Pr_0 flow, yields a length scale $y_s \sim \delta_v$ and mean velocity scale $U_s \sim \eta_T \Delta T\, u_s$ [as per Eq. (22)]. The corresponding time-averaged friction factor scales as

$$\bar{\tau}_w = \frac{(\tau_w)_{\mathrm{avg}}}{\rho_0 U_s^2} \sim \frac{\nu_0}{U_s\, \delta_v} \sim \frac{\nu_0}{\eta_T\, \Delta T\, u_s \sqrt{\mathrm{Pr}_0} \delta_t} \sim \frac{\mathrm{Pr}_0^{1/2}}{\beta_T\, \eta_T\, (\Delta T)^2}. \tag{24}$$

Thus, for both high-Pr_0 and low-Pr_0 flows, the friction factor is independent of wavelength and speed of the temperature wave and is inversely proportional to the dimensionless "thermoviscous actuation parameter," $\beta_T\, \eta_T\, (\Delta T)^2$. The summary of the scaling analysis is presented in Table I.

IV. ASSESSMENT WITH NUMERICAL SIMULATION RESULTS

In order to corroborate the scaling estimates for viscous penetration depth and time-averaged velocity, we perform a full-scale numerical solution of the pertinent governing equations [Eqs. (2), (3), and (4)] for a wide range of mean Prandtl numbers (Pr_0). The geometry comprises a rectangular domain ($L \times H$) with both $L, H \gg \lambda$. Here, L represents the x dimension (along the flat wall) and H stands for the y dimension (normal to the wall). The wall ($y = 0$) is subjected to a no-slip condition for flow equations and a traveling temperature wave thermal boundary condition as dictated by Eq. (1). Far away from the wall ($y = H$), velocities, temperature, and pressure are bounded ($u = v = 0$, $T = T_0$, and $p = p_{\mathrm{atm}}$). Since the length scales (λ, δ_t, etc.) are very small, we need a high-resolution grid for the simulations. In order to resolve the boundary layer region accurately, the computational domain is meshed with a nonuniform rectangular grid which is sufficiently refined near the wall. Typically, a flow domain having size $L = 2$ mm and $H = 5$ mm has 2.67×10^5 computational cells (found to be sufficient after a grid independence study). Since the time scale (λ/c) is extremely small too, a quad core Xeon CPU (clock speed 3.5 GHz) takes about 150 hours to solve for just 0.1 second flow time.

The governing equations are discretized on the nonuniform mesh using a fully implicit, control volume based finite difference technique. The third-order accurate QUICK (Quadratic Upstream Interpolation for Convective Kinematics) scheme is employed for the convective terms in momentum and energy equations. Pressure-velocity coupling is achieved via the Semi-Implicit Method for Pressure Linked Equations (SIMPLE) algorithm. In order to solve the discretized system of linear algebraic equations, we utilize a point implicit (Gauss-Seidel) solver. Detailed descriptions of these numerical techniques are available in Patankar [37] and Versteeg and Malalasekera [38]. Since the formulation is fully time implicit, the solution is unconditionally stable irrespective of the time step size. Nevertheless, considering the physics of the problem, we select the time step size(s) based on the periodic time scale $t_u (=\lambda/c)$. An extensive mesh and time step dependency analysis has been carried out, and a time step size of order $\sim 0.01(\lambda/c)$ is found to be adequate. In order to be time accurate, the iteration process is continued till convergence within each time step. The convergence

TABLE II. Thermophysical properties of mercury, water, and ethylene glycol [39,40].

Parameter (unit)	Mercury (at $T_0 = 77\,^\circ$C)	Water (at $T_0 = 30\,^\circ$C)	Ethylene glycol (at $T_0 = 47\,^\circ$C)
ρ_0(kg/m^3)	13407	995.5	1096.2
μ_0 (Pa s)	1.31×10^{-3}	8×10^{-4}	7.57×10^{-3}
β_T(K^{-1})	1.81×10^{-4}	2.97×10^{-4}	6.5×10^{-4}
η_T(K^{-1})	0.0026	0.0215	0.0316
$\alpha_0 = k_0/\rho_0 C_p$(m^2/s)	4.97×10^{-6}	1.47×10^{-7}	9.4×10^{-8}
Pr_0	0.0196	5.43	73.5

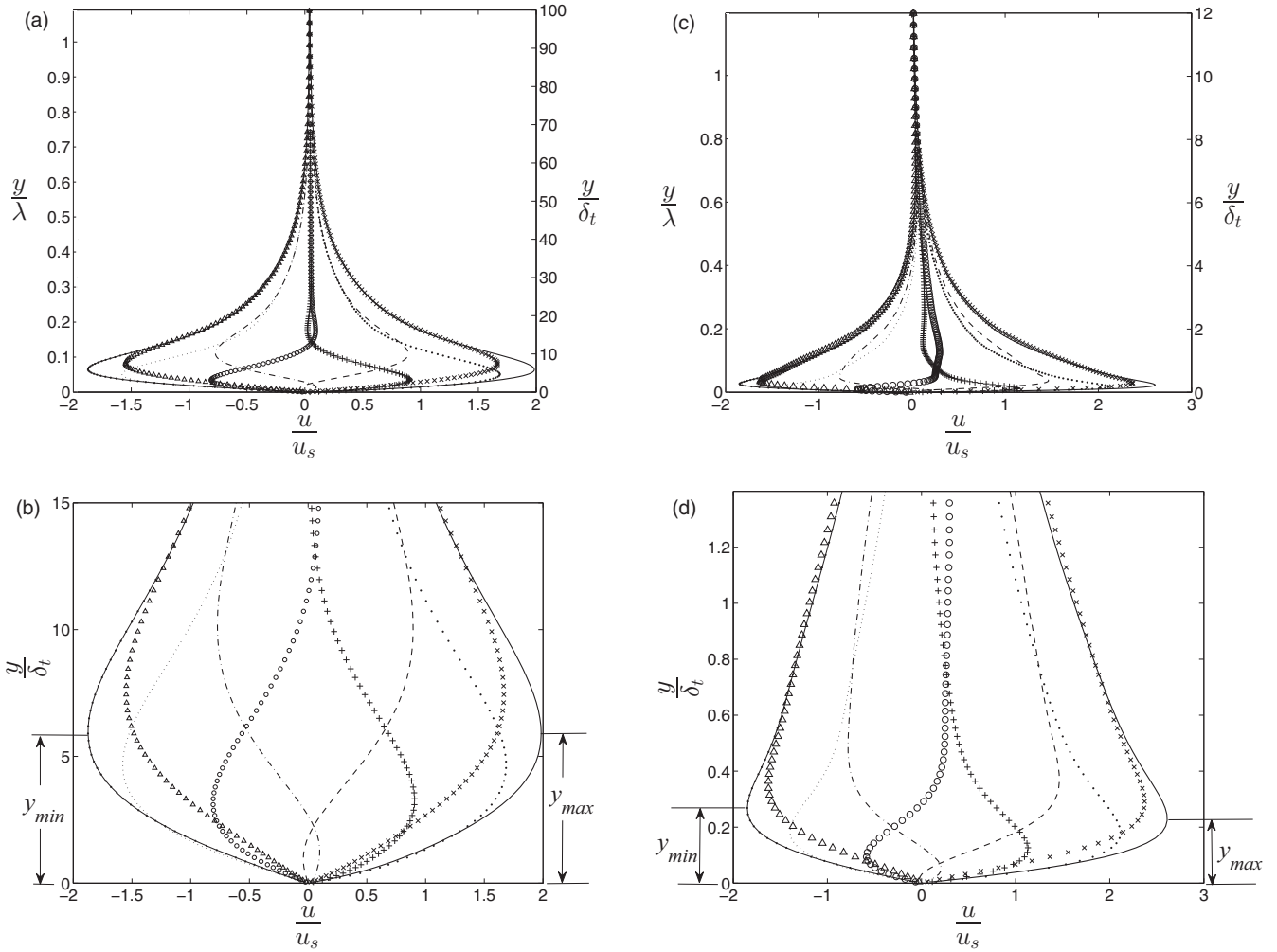

FIG. 2. Oscillation of normalized x velocity during the course of one cycle (time period $t_u = \lambda/c$). Every figure depicts ten velocity profiles capturing ten different instants of the cycle at equal time interval of $0.1t_u$. (a) $\mathrm{Pr}_0 = 54$ case; (b) enlarged view of the velocity profiles in (a) near the wall; (c) $\mathrm{Pr}_0 = 0.054$ case; (d) magnified view of the velocity profiles in (c) near the wall.

criteria for the maximum relative error are set as 10^{-6}, for all the discretized equations. Temperature-dependent density and viscosity are updated through linearized relations (5) and (6). Thermophysical properties of mercury, water and ethylene glycol are used as input data for three particular cases, with $\mathrm{Pr}_0 = 0.0196$, 5.43, and 73.5, respectively (see Table II). For the rest of the cases, mean Prandtl number is varied by altering the viscosity (μ_0) and/or the thermal conductivity value (k_0) of water. Such an alteration is acceptable for the purpose of verification of the scaling laws under concern. The restriction of $\lambda/\delta_t \geqslant 10$ is maintained throughout. The mean velocity field is obtained by time averaging u and v at every point (cell) of the computational domain.

A. Illustrations of flow field and viscous boundary layer

In an effort to validate the scaling law developed for the viscous penetration depth, several cases with distinct high and low Pr_0 values are considered. For each case, variations of instantaneous x velocity (u), normalized with respect to u_s [expression (7)], are monitored over one complete cycle (time period $t_u = \lambda/c$). Figures 2(a) and 2(b) demonstrate the oscillation of u at a given x location for one such high-Pr_0 case ($\mathrm{Pr}_0 = 54$). Time instants when u reaches its peaks (positive peak u^+_{max} and negative peak u^-_{min}) are also captured in these figures [see left- and rightmost profiles in Fig. 2(b)]. Corresponding plots of dimensionless x velocity for a low-Pr_0 case ($\mathrm{Pr}_0 = 0.054$) are presented in Figs. 2(c) and 2(d). The averaged y coordinates of peak x velocities (u^+_{max} and u^-_{min}), as determined from the numerical solution, are $\delta_v \approx 5.9\delta_t$ and $\delta_v \approx 0.24\delta_t$, respectively, for $\mathrm{Pr}_0 = 54$ and $\mathrm{Pr}_0 = 0.054$ cases. These profiles clearly show that the exact location where x velocity reaches its peak depends on the Prandtl number. The viscous boundary layer thickness (δ_v) thus depends not only on the extent of thermal diffusion (and subsequent expansion-contraction of the fluid) but also on the Prandtl number. The difference between dimensionless $|u^+|$ and $|u^-|$ is substantial in the low-Pr_0 case as compared to the high-Pr_0 case, as demonstrated in Fig. 2. In each case, all the x-velocity profiles belonging to a same cycle (usually of very small time period, $t_u \sim 10^{-4}$ s) eventually merge to a single value of u at around $y \sim \lambda$, as evident from Figs. 2(a) and 2(c). In other words,

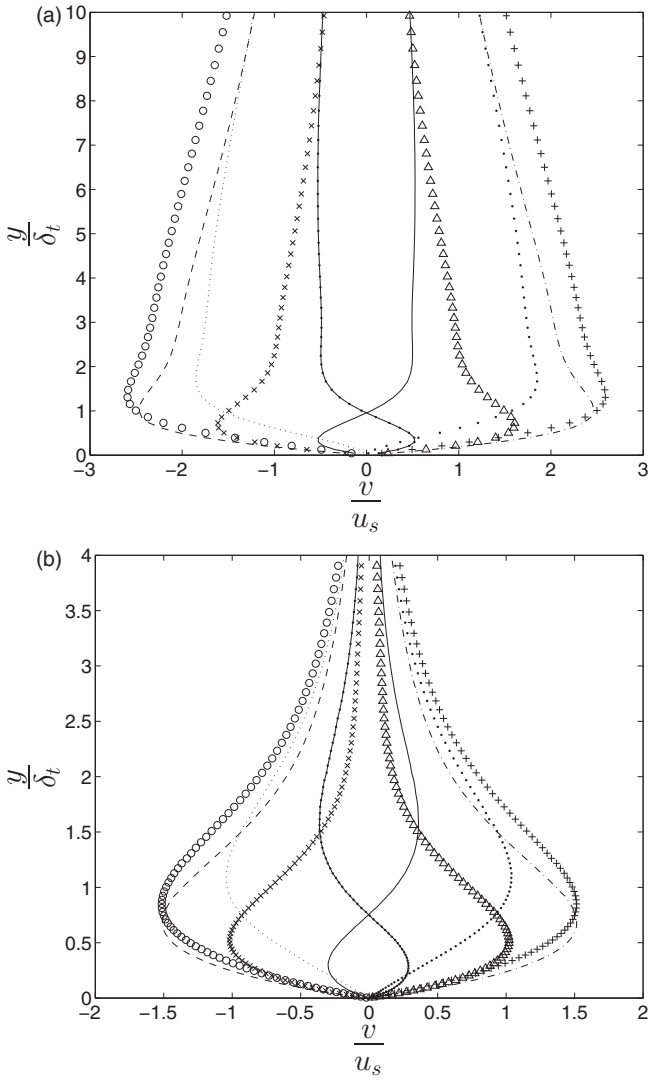

FIG. 3. Oscillation of dimensionless y velocity during the course of one cycle (time period $t_u = \lambda/c$). Every figure depicts ten velocity profiles capturing ten different instants of the cycle at equal time interval of $0.1t_u$. (a) $\mathrm{Pr}_0 = 54$ and (b) $\mathrm{Pr}_0 = 0.054$. Note the symmetry of the profiles about the midpoint ($v = 0$), which actually demonstrates that the mean transverse velocity $V_{\mathrm{avg}} = 0$ in the entire domain, irrespective of the Prandtl number.

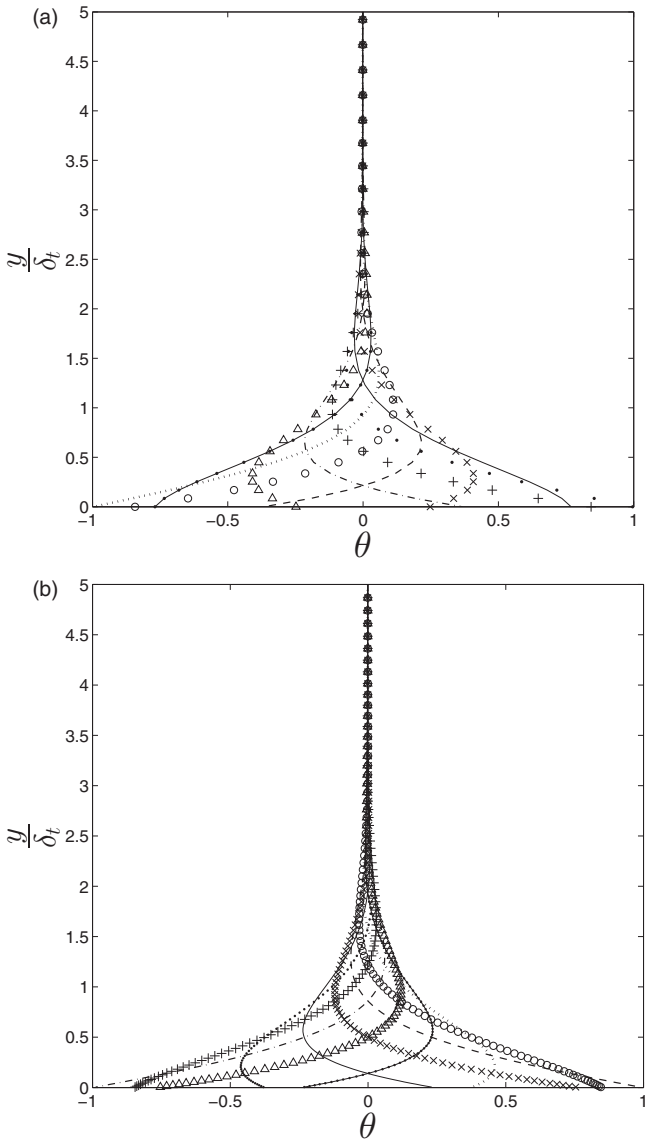

FIG. 4. Oscillation of dimensionless temperature $\theta = (T - T_0)/\Delta T$ during the course of one cycle (time period $t_u = \lambda/c$). Every figure depicts ten temperature profiles capturing ten different instants of the cycle at equal time intervals of $0.1t_u$. (a) $\mathrm{Pr}_0 = 54$ and (b) $\mathrm{Pr}_0 = 0.054$. Note that the extents of thermal boundary layer are the same ($\simeq 2.66\,\delta_t$) for both the Prandtl numbers ($\mathrm{Pr}_0 = 54$ and 0.054), which are obtained by altering the thermal conductivity of water.

oscillation of u decays gradually outside the viscous boundary layer ($y > \delta_{\mathrm{v}}$) and stops completely at $y \simeq \lambda$.

The oscillations of dimensionless y velocity and temperature during a cycle are depicted in Figs. 3 and 4, respectively. Figures 3(a) and 4(a) represent the same high-Pr_0 case ($\mathrm{Pr}_0 = 54$) as in Fig. 2(a). Figures 3(b) and 4(b) correspond to the low-Pr_0 case ($\mathrm{Pr}_0 = 0.054$) as in Fig. 2(c). It is evident that the y component of velocity (v) attains its peak at around $y_s \sim \delta_t$, irrespective of the Prandtl number. Oscillation of v decays gradually outside the thermal boundary layer (wall layer) and becomes zero at around $y \sim \lambda$. In both high-Pr_0 and low-Pr_0 cases, temperature fluctuation is confined within the wall layer. It is clear that the fluctuation of v is solely governed by inertia outside the wall layer, regardless of the Prandtl number.

B. Assessment of the scaling laws for δ_{v}

Figure 5 portrays numerically obtained viscous boundary layer thickness (δ_{v}) relative to thermal penetration length (δ_t) for a wide range of Pr_0. The straight lines in Fig. 5 are drawn to represent same slope ($=\frac{1}{2}$). The CFD solution captures the trends prescribed by relations (15) and (18) well, except for the situations where the Prandtl numbers are very high (say, $\mathrm{Pr}_0 > 100$). In a low Reynolds number flow, it is not completely surprising that the ratio of viscous and thermal spreading lengths scales as $\sqrt{\mathrm{Pr}}$, irrespective of the Prandtl number under concern [41]. While the present result is consistent with such fundamental principle, it must be noted

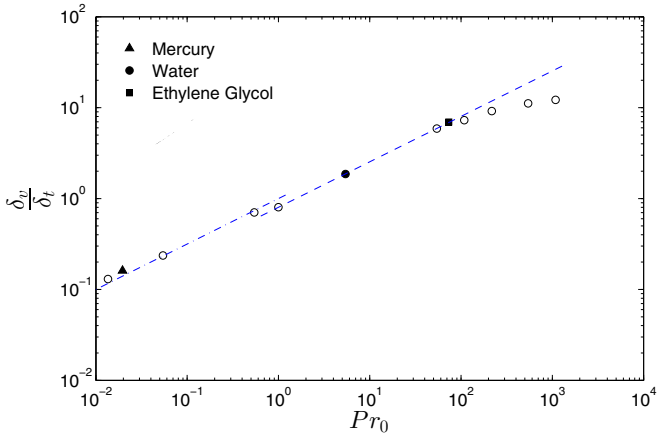

FIG. 5. Variation of viscous boundary layer thickness relative to thermal boundary layer thickness for a wide range of mean Prandtl numbers. White circles represent CFD simulation data for water with changed values of mean viscosity and/or thermal conductivity. Since Pr_0 is increased beyond 100 by increasing the viscosity (keeping λ the same), the dependence of viscous boundary layer thickness (δ_v) on Pr_0 decreases substantially.

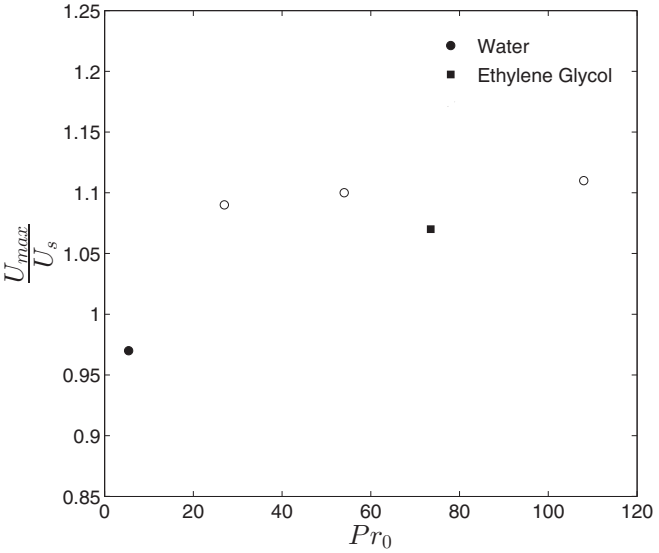

FIG. 6. Maximum mean velocity (normalized) vs Prandtl number in the high-Pr_0 regime. Mean velocity scale U_s is taken from Eq. (21). White circles represent CFD solutions for water with modified values of mean viscosity and/or thermal conductivity.

that the scale $\delta_\mathrm{v}/\delta_t \sim \mathrm{Pr}_0^{1/2}$ may fail in a high-Pr_0 regime as depicted in Fig. 5. When Pr_0 is raised beyond a stipulated value by increasing the mean viscosity (μ_0), the extent of the viscous boundary layer (δ_v) is restricted by the wavelength λ and the $\delta_\mathrm{v}/\delta_t$ ratio becomes less and less dependent on Pr_0. Note that in an unconfined environment the characteristic y length scale for the variation of x velocity is the wavelength λ [see Figs. 2(a) and 2(c)]. If we increase Pr_0 by decreasing thermal conductivity only, then the scale $\delta_\mathrm{v}/\delta_t \sim \mathrm{Pr}_0^{1/2}$ is maintained. Another important point is that the scaling laws (15) and (18) are applicable for a Pr_0 value somewhat greater or lesser than unity as well, even though they were established considering the limiting cases of $\mathrm{Pr}_0 \gg 1$ and $\mathrm{Pr}_0 \ll 1$.

C. Assessment of mean flow

In this section, we explore some important and interesting features of the time-averaged (mean) flow field. For high-Pr_0 fluids, the streamwise mean velocity (U_avg) reaches its peak or maximum (U_max) within the thermal boundary layer, at around $y \approx \delta_t$. We recall that it is the thermal boundary layer ($\sim\delta_t$) wherein the periodic fluctuation of temperature and associated thermoviscous actuation remain confined. In order to assess the mean velocity scale [Eq. (21)], we plot the normalized U_max against Pr_0 in Fig. 6. As expected, U_max normalized by the appropriate scale [expression (21)] yield values close to 1 for different Pr_0 (=5.43, 27, 54, 73.5, 108, etc.).

One of the most interesting findings of the present study is the seemingly nontrivial mean velocity distribution originating out of thermoviscous expansion of low Prandtl number fluids. For low-Pr_0 flows, we observe a sharp rise and a subsequent sharp fall (albeit smaller extent) of the mean velocity near the wall, as depicted in Fig. 7(a). A "steady" velocity distribution with a local spike or overshoot close to the wall [Fig. 7(a)] is not so common in nature. The physics behind such behavior relies on the intricate interplay among distinctive length scales (δ_v and δ_t), local velocity gradient, and temperature phase difference.

To figure out the peculiarity in the mean velocity profile, one needs to examine the temperature field near the wall, the instantaneous x-velocity gradient during an entire cycle [e.g., Fig. 2(d)], and the mean flow governing equation [Eq. (19)] carefully. Noting that $\delta_\mathrm{v} \ll \lambda$, the mean flow governing equation [Eq. (19)] may be simplified as

$$\frac{\partial^2 U_\mathrm{avg}}{\partial y^2} \simeq \eta_T \frac{\partial}{\partial y}\left[\overline{(T-T_0)\left(\frac{\partial u}{\partial y}\right)}\right]. \tag{25}$$

In order to examine the temperature field, it is necessary to recall the structure of the thermal boundary layer [25] that is divided into two sublayers depending on the phase difference in local temperature: (a) a wall-inner sublayer ($0 \leqslant y \leqslant \delta^*/3 \simeq 0.9\,\delta_t$) in which temperature deviation $(T - T_0)$ has the same sign as the local $(T_w - T_0)$, and (b) a wall-outer sublayer ($\delta^*/3 < y \leqslant \delta^*$) wherein temperature deviation $(T - T_0)$ has sign opposite to the local $(T_w - T_0)$. Here, T_w is the local wall temperature and δ^* is the exact thickness of the thermal boundary layer (obtained from an analytical solution of the temperature field [25]). When δ_v is smaller than the thickness of the wall-inner sublayer ($\delta^*/3 \simeq 0.9\,\delta_t$), e.g., the $\mathrm{Pr}_0 = 0.054$ case in which $\delta_\mathrm{v} \approx 0.24\,\delta_t$ [Fig. 7(a)], one can split the wall-inner sublayer into two parts: the viscous boundary layer ($0 \leqslant y \leqslant \delta_\mathrm{v}$) region and the $\delta_\mathrm{v} < y \leqslant \delta^*/3$ region. In the viscous boundary layer, the interaction of local temperature deviation $(T - T_0)$ and velocity gradient $\partial u/\partial y$ is congenial for generating a positive and substantially large thermoviscous force, which leads to a steep rise in U_avg till $y \sim \delta_\mathrm{v}$. In the region $\delta_\mathrm{v} < y \leqslant \delta^*/3$, the temperature field is still favorable, but the local $\partial u/\partial y$ has changed in various aspects. Here, the velocity gradient does not scale as $\partial u/\partial y \sim u_s/\delta_\mathrm{v}$ and its sign has changed too, as is evident from Fig. 2(d). Not only is the sign of $\partial u/\partial y$ opposite, but its

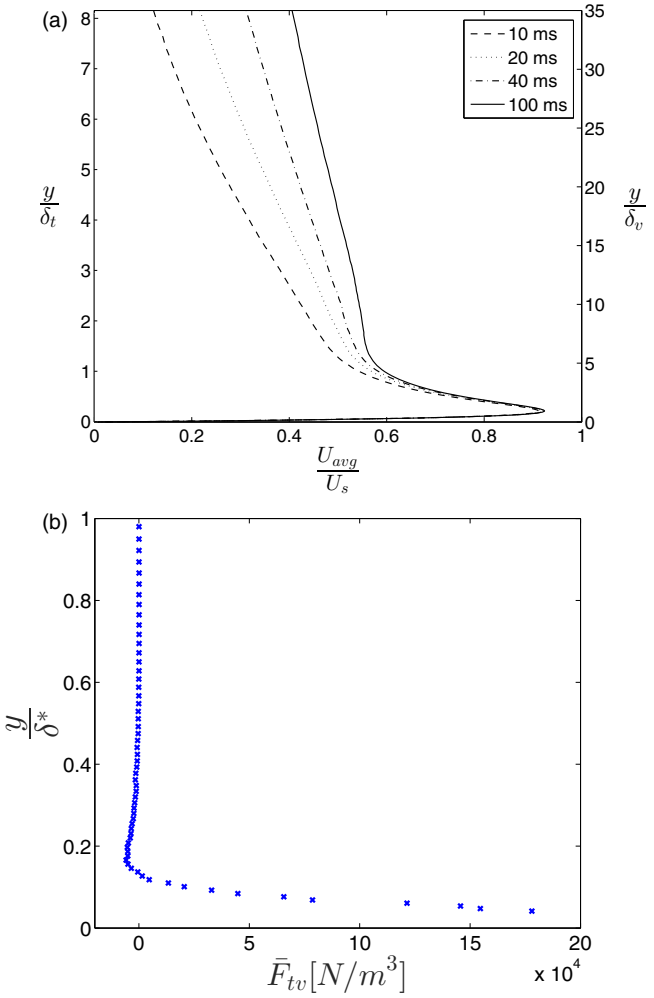

FIG. 7. (a) Time evolution of mean velocity profile near the wall for a low Prandtl number ($\mathrm{Pr}_0 = 0.054$) case. Mean velocity scale U_s is taken from Eq. (22). (b) Net thermoviscous force distribution over the flat plate at $t = 100$ ms for the same case ($\mathrm{Pr}_0 = 0.054$). Here, $\delta^* \simeq 2.7\delta_t$ and $\delta_v \simeq 0.24\,\delta_t$. To show the negative force zone, the force axis (horizontal) is clipped.

magnitude $|\partial u/\partial y|$ is considerably less than that in the viscous boundary layer region. All these factors contribute towards a decrement in U_{avg} with y in the $\delta_v < y \leqslant \delta^*/3$ layer at a smaller rate. Eventually, U_{avg} settles down to a lower value at around $y \simeq \delta^*/3$ (the edge of the wall-inner sublayer). Thus, the instantaneous velocity gradient in $\delta_v < y \leqslant \delta^*/3$ zone adversely affects the thermoviscous actuation and hinders generation of net flow by reducing the mean velocity. In the wall-outer sublayer ($\delta^*/3 < y < \delta^*$), however, both $(T - T_0)$ and $\partial u/\partial y$ possess opposite sign and their combination results in a positive thermoviscous force [although it is substantially weaker since the magnitude of $(T - T_0)$ is small compared to that in the wall-inner sublayer]. Outside the thermal boundary layer ($y > \delta^*$), thermoviscous force is zero and the mean velocity is time dependent.

To sum up, the mean velocity distribution within the wall layer is dictated by a balance between viscous drag and local thermoviscous force. Close to the wall ($y \sim \delta_t$) mean flow remains steady. The net thermoviscous force distribution, presented in Fig. 7(b), only confirms the phenomena described above. It is the negative thermoviscous force that draws the mean flow back even within the thermal boundary layer [till $y \sim \delta^*/3 \simeq 0.9\delta_t$, as demonstrated in Fig. 7(a)]. These results conclusively prove that the thermoviscous force function within the wall layer or thermal boundary layer need not be a monotonically decreasing one. In reality, it depends on the ratio of viscous penetration depth to thermal penetration length, which essentially controls the magnitude and sign of local temperature deviation as well as the local velocity gradient. In this particular case ($\mathrm{Pr}_0 = 0.054$), the force function becomes (slightly) positive again in the wall-outer sublayer, before eventually going down to zero around $y \simeq \delta^*$. Thus, the negative thermoviscous force can substantially reduce the net mass flow rate along the plate even though the Prandtl number is small ($\mathrm{Pr}_0 \ll 1$).

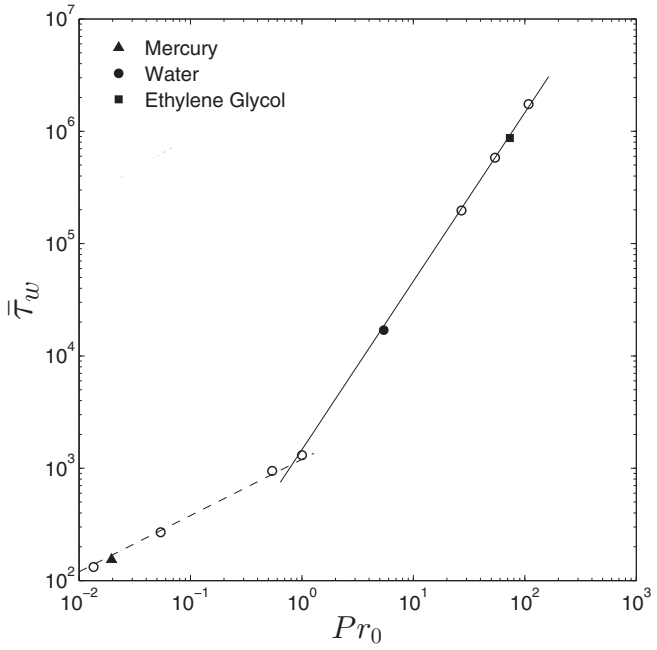

FIG. 8. Dimensionless wall shear (time-averaged) variation with Prandtl number for a constant $\beta_T \eta_T (\Delta T)^2$. White circles represent CFD simulation data for water with changed values of mean viscosity and/or thermal conductivity. Lines simply represent slopes ($\frac{1}{2}$ and $1\frac{1}{2}$).

D. Friction factor variation with Prandtl number

Figure 8 presents numerically obtained friction factor (dimensionless wall shear), plotted against the mean Prandtl number keeping 'thermoviscous actuation parameter' constant ($\beta_T \eta_T \Delta T^2 = 2.555 \times 10^{-3}$). Straight lines are drawn in the same figure to represent different slopes – the dashed line has a slope = ½ (low-Pr_0 regime), while the solid continuous line has a slope = 1½ (high-Pr_0 regime). The agreement between scaling estimates and simulation results (data points) are excellent. In addition, numerical result demonstrates that the scales for the friction factor are also valid for a Pr_0 that is moderately higher or lower than unity.

V. CONCLUSIONS

In this paper, we have developed scaling relationships for the limiting cases of large Prandtl number ($Pr_0 \gg 1$) and small Prandtl number ($Pr_0 \ll 1$) flows induced by thermoviscous expansion of a liquid along a traveling temperature wave. Employing full-scale CFD simulations, we not only corroborate the scaling laws but demonstrate that these laws are also applicable to Prandtl numbers moderately higher and lower than unity, widening their ranges of validity. We show that deviation of mean Prandtl number (Pr_0) from unity introduces a viscous length scale (δ_v) which, relative to the thermal penetration length (δ_t), scales as $\sim Pr_0^{1/2}$, irrespective of the regime of Prandtl number (Pr_0) under concern. There is, however, a constraint on this seemingly universal scale: it is valid as long as viscous penetration depth (δ_v) remains small compared to the wavelength of the applied thermal wave (λ).

Investigation of mean (time-averaged) flow reveals an intriguing aspect of thermoviscous actuation. Here, we have demonstrated that the thermoviscous force can remarkably be negative within the thermal boundary layer itself, particularly for low Pr_0 ($\ll 1$) flows, leading to a nontrivial reduction of net (time-averaged) throughput along the wall. Such a nontrivial mean flow pattern (mean velocity distribution) is attributed to the intricate interplay of viscous length scale (δ_v) and different sublayers of the thermal boundary layer.

The scaling and numerical investigations are further extended towards unveiling the friction factor (dimensionless wall shear) characteristics for high-Pr_0 and low-Pr_0 fluids. Numerical prediction of friction factor variation with Prandtl number agrees well with the scaling estimates for both high-Pr_0 and low-Pr_0 fluids. It is found that the thermoviscous actuation parameter, $\beta_T \eta_T \Delta T^2$, always (for all Pr_0) augments the mean velocity, curbing the friction factor.

Our scaling estimates effectively bring out the essential physics of interest, without necessitating expensive numerical simulations, pertaining to thermoviscous expansion on a flat plate on which a traveling temperature wave recurs in a spatiotemporally evolving manner. Many extended implications of the present scaling analysis can be applied to address transport phenomena in several other applications ranging from microfluidics to the processing of materials [42–54]. Results obtained from the present study will also be useful in the area of thermal molecular focusing and ultrasound acoustophoresis. The process of trapping, accumulation, and sorting of colloidal particles and biomolecules with frequency-tunable control may be improved through proper knowledge of fundamental physical scales associated with thermoviscous flow actuation.

ACKNOWLEDGMENTS

S.C. acknowledges the Department of Science and Technology, Government of India, for support through a Sir J. C. Bose National Fellowship. D.P. acknowledges the Indian National Academy of Engineering for fellowship support.

[1] H. A. Stone, A. D. Stroock, and A. Ajdari, Annu. Rev. Fluid Mech. **36**, 381 (2004).
[2] M. W. J. Prins, W. J. J. Welters, and J. W. Weekamp, Science **291**, 277 (2001).
[3] M. G. Pollack, R. B. Fair, and A. D. Shenderov, Appl. Phys. Lett. **77**, 1725 (2000).
[4] T. S. Sammarco and M. A. Burns, AIChE J. **45**, 350 (1999).
[5] D. A. Saville, Annu. Rev. Fluid Mech. **9**, 321 (1977).
[6] R. Hunter, *Zeta Potential in Colloid Science: Principles and Applications* (Academic, London, 1981).
[7] S. Ghosal, Annu. Rev. Fluid Mech. **38**, 309 (2006).
[8] N. G. Green, A. Ramos, A. González, H. Morgan, and A. Castellanos, Phys. Rev. E **61**, 4011 (2000).
[9] A. Ramos, H. Morgan, N. G. Green, A. González, and A. Castellanos, J. Appl. Phys. **97**, 084906 (2005).
[10] A. González, A. Ramos, H. Morgan, N. G. Green, and A. Castellanos, J. Fluid Mech. **564**, 415 (2006).
[11] N. Riley, Annu. Rev. Fluid Mech. **33**, 43 (2001).
[12] J. C. Rife, M. I. Bell, J. S. Horwitz, M. N. Kabler, R. C. Y. Aeuyeung, and W. J. Kim, Sens. Actuators A **86**, 135 (2000).
[13] G. Zabow, F. Assi, R. Jenks, and M. Prentiss, Appl. Phys. Lett. **80**, 1483 (2002).
[14] Z. Yang, H. Goto, M. Matsumoto, and R. Maeda, Electrophoresis **21**, 116 (2000).
[15] H. H. Bau, J. H. Zhong, and M. Q. Yi, Sens. Actuators B **79**, 207 (2001).
[16] N. T. Nguyen, X. Huang, and T. K. Chuan, J. Fluids Eng. **124**, 384 (2002).
[17] D. E. Kataoka and S. M. Troian, Nature (London) **402**, 794 (1999).
[18] B. S. Gallardo, V. K. Gupta, F. D. Eagerton, L. I. Jong, V. S. Craig, R. R. Shah, and N. L. Abbott, Science **283**, 57 (1999).
[19] E. Yariv and H. Brenner, Phys. Fluids **16**, L95 (2004).
[20] F. M. Weinert, J. A. Kraus, T. Franosch, and D. Braun, Phys. Rev. Lett. **100**, 164501 (2008).
[21] Q. Yuan and J. Wu, Biomed. Microdevices **15**, 125 (2013).
[22] S. J. Williams, Electrophoresis **34**, 1400 (2013).
[23] S. J. Williams and N. G. Green, Electrophoresis **36**, 1681 (2015).
[24] C. Zhang, H. Wong, and K Nandakumar, J. Fluid Mech. **848**, 1040 (2018).
[25] D. Pal and S. Chakraborty, Phys. Fluids **27**, 053601 (2015).
[26] D. Pal and S. Chakraborty, Phys. Rev. E **86**, 016321 (2012).
[27] A. Y. Rednikov and S. S. Sadhal, J. Fluid Mech. **667**, 426 (2011).
[28] P. B. Muller and H. Bruus, Phys. Rev. E **90**, 043016 (2014).
[29] P. B. Muller and H. Bruus, Procedia IUTAM **10**, 410 (2014).
[30] N. Osterman and D. Braun, Appl. Phys. Lett. **106**, 073508 (2015).
[31] T. Fukuyama, S. Nakama, and Y. T. Maeda, Soft Matter **14**, 5519 (2018).

[32] D. C. Walther and J. Ahn, Prog. Energy Combust. Sci. **37**, 583 (2011).
[33] K. Maruta, Proc. Combust. Inst. **33**, 125 (2011).
[34] S. K. Chou, W. M. Yang, K. J. Chua, J. Li, and K. L. Zhang, Appl. Energy **88**, 1 (2011).
[35] A. Tripathi, O. Bozkurt, and A. Chauhan, Phys. Fluids. **17**, 103607 (2005).
[36] D. Pal and S. Chakraborty, Proc. R. Soc. A **475**, 20190382 (2019).
[37] S. V. Patankar, *Numerical Heat Transfer and Fluid Flow* (McGraw-Hill, New York, 1980).
[38] H. Versteeg and W. Malalasekera, *An Introduction to Computational Fluid Dynamics: The Finite Volume Method* (Prentice Hall, London, 2007).
[39] A. Bejan, *Convection Heat Transfer* (Wiley, New York, 1995).
[40] T. L. Bergman, A. S. Lavine, F. P. Incropera, and D. P. Dewitt, *Fundamentals of Heat and Mass Transfer* (Wiley, New York, 2011).
[41] F. M. White, *Viscous Fluid Flow* (McGraw-Hill, New York, 2005).
[42] R. P. Kate, P. K. Das, and S. Chakraborty, J. Fluid Mech. **573**, 247 (2007).
[43] S. Chakraborty and S. K. Som, Int. J. Heat Mass Transfer **48**, 2801 (2005).
[44] S. Das, T. Das, and S. Chakraborty, Sens. Actuators B **114**, 957 (2006).
[45] A. Bandopadhay, D. Tripathi, and S. Chakraborty, Phys. Fluids **28**, 052002 (2016).
[46] S. Das, S. Chakraborty, and S. K. Mitra, Phys. Rev. E **85**, 051508 (2012).
[47] S. Chakraborty and S. Ray, Phys. Fluids **20**, 083602 (2008).
[48] S. Das and S. Chakraborty, AIChE J. **53**, 1086 (2007).
[49] A. Garai and S. Chakraborty, Electrophoresis **31**, 843 (2010).
[50] S. P. Das, S. Chakraborty, and P. Dutta, Heat Transfer Eng. **25**, 54 (2004).
[51] S. Chakraborty, Appl. Phys. Lett. **90**, 034108 (2007).
[52] S. Sarkar, P. M. Raj, S. Chakraborty, and P. Dutta, Numer. Heat Transfer, Part A **42**, 307 (2002).
[53] P. M. Raj, S. Sarkar, S. Chakraborty, G. Phanikumar, and P. Dutta, Int. J. Heat Fluid Flow **23**, 298 (2002).
[54] P. Goswami, J. Chakraborty, A. Bandopadhyay, and S. Chakraborty, Microvasc. Res. **103**, 41 (2016).